Clinics in Oncology

Research Article
Published: 24 Aug, 2023

A Cuproptosis-Related lncRNAs Risk Model to Predict Prognosis and Immune Characteristics in Breast Cancer

Xu XY[1,2†], Song YH[3†], Liu XQ[5] and Lin XY[1,4*]*

[1]Department of Pathology, Shandong Provincial Hospital, Shandong First Medical University, China

[2]College of Basic Medicine, Shandong First Medical University-Shandong Academy of Medical Sciences, China

[3]Department of Pulmonary and Critical Care Medicine, Shandong Second Provincial General Hospital, Shandong University, China

[4]Department of Pathology, Shandong Provincial Hospital, Shandong University, China

[5]Department of Breast Disease Diagnosis and Treatment Center, Central Hospital, Shandong First Medical University, China

[†]These authors are contributed equally to this work

Abstract

Background: Cuproptosis (copper death) is a newly-rising research field in cell death, which is not completely elucidated when it comes to bioinformatics studies of Breast Cancer (BRCA). In this study, we aimed to discover cuproptosis-Related Long noncoding RNA (CRLs) and construct a prognostic risk model, particularly related to the immune characteristics with the goal of providing potential therapeutic guidelines for clinical treatment.

Methods: Based on the cancer genome Atlas-BRCA transcriptome data, top five CRLs were screened, and Pearson's correlation was used to identify CRLs. Then we applied least absolute shrink age and selection operator Cox regression, and univariate Cox analysis to construct a prognostic risk model. Additionally, immune cells and immune checkpoints between risk groups were identified using the CIBERSORT. Finally, five CRLs were identified as the ultimate prognostic factors using the quantitative Reverse Transcription-Polymerase Chain Reaction (qRT-PCR) method.

Results: The risk score and age can act as independent diagnostic factors in the prognostic risk model with a shorter overall survival time detected in the high-risk group. Immune cells and immune checkpoints between high- and low-risk groups showed a significant difference. Finally, we observed that AC092718.4 expression in three cell lines and clinical tissues was up-regulated, while AL050343.1, AL590434.1, AC105398.1 and AP001021.1 expression were down-regulated.

Conclusion: The five prognostic CRLs have the potential to forecast prognosis and promote clinical drug selection, providing a theoretical foundation for clinical treatment.

Keywords: Bioinformatics analysis; Breast cancer; Cuproptosis-related lncRNA; Risk model; Prognosis; Immune microenvironment

OPEN ACCESS

Correspondence:
Xianqiang Liu, Department of Breast Disease Diagnosis and Treatment Center, Central Hospital Affiliated to Shandong First Medical University, Jinan, China
Xiaoyan Lin, Department of Pathology, Shandong Provincial Hospital Affiliated to Shandong First Medical University, Jinan, 250021, China

Received Date: *22 Jul 2023*
Accepted Date: *06 Aug 2023*
Published Date: *24 Aug 2023*

Citation:
Xu XY, Song YH, Liu XQ, Lin XY. A Cuproptosis-Related lncRNAs Risk Model to Predict Prognosis and Immune Characteristics in Breast Cancer. Clin Oncol. 2023; 8: 2010.

ISSN: 2474-1663

Introduction

As of 2022, Breast Cancer (BRCA) has the highest estimated incidence and second highest projected mortality among all cancers in females worldwide; it comprises three subtypes: Luminal BRCA, human epidermal growth factor receptor 2-positive BRCA, and Triple-Negative Breast Cancer (TNBC) [1,2]. Despite constant advances in radiotherapy, chemotherapy, surgical resection, and immune checkpoint blockers, therapeutic efficacy remains unsatisfactory due to tumour heterogeneity [3-5]. Owing to the various subtypes, complex pathogenesis, high recurrence rate, and increased drug resistance, more theoretical research is required to provide cutting-edge treatment for breast cancer in clinical practice.

Copper is a trace element essential for life and is involved in various human biological processes, including maintenance of haematopoiesis, nervous system protection, resistance to oxidation, and participation in mitochondrial respiration [6]. Despite being an indispensable cofactor, copper could cause cytotoxicity. Copper is directly involved in the tricarboxylic acid cycle and binds with lipoylated molecules to promote Iron (Fe)-Sulphur (S) cluster protein loss, resulting in cell death [7]. Elesclomol is a potent copper ionophore and promotes cuproptosis (copper death). Elesclomol

specifically binds Ferredoxin 1 (*FDX1*) α2/α3 helices and the β5 strand. It also inhibits *FDX1*-mediated Fe-S cluster biosynthesis. Being an oxidative stress inducer, it induces cancer cell apoptosis. Cuproptosis is a novel programmed cell death that differs from apoptosis, necroptosis, pyroptosis, immunogenic cell death, and ferroptosis [8,9].

Long noncoding Ribonucleic Acid (RNA) (lncRNA) was first reported in 1991, with X-inactive specific transcript regulating X-chromosome inactivation [10]. lncRNAs measure >200 nucleotides in length, are mainly distributed in the nucleus and are involved in various biological processes, including cellular development, cellular drug resistance, and immune microenvironment regulation [11]. Similar studies have reported that abnormal lncRNA expression is associated with multiple malignant tumours, including BRCA [12,13]. However, Cuproptosis-Related lncRNAs (CRLs) in BRCA have not been reported in the literature.

In this study, five CRLs were identified, and risk prognosis models were constructed based on The Cancer Genome Atlas (TCGA) database. We estimated the relationship between the risk model and the immune microenvironment, functional enrichment, and drug sensitivity. This model could well predict the Overall Survival (OS) and might provide a new strategy for clinical treatment.

Materials and Methods

Data acquisition

Transcriptome data for BRCA, including 112 normal cases and 1100 tumour cases, were downloaded from TCGA (http://portal.gdc.cancer.gov/). The corresponding clinical information and single-nucleotide variation were also obtained from TCGA. Cuproptosis-Related Genes (CRGs) were obtained in a previous study [8]. Herein, we only collected data for females.

Identification of CRLs and construction of a risk prognosis model

CRLs were obtained using Pearson's correlation algorithm (|cor| >0.45, p<0.001). The relationship between CRGs and CRLs was analysed using R software. Univariate Cox (Uni-Cox) analysis was applied to screen prognosis-related CRLs (p<0.05). The best prognosis-related CRLs were filtered using the Least Absolute Shrinkage and Selection Operator Cox (LASSO-Cox) algorithm. Then, the TCGA-BRCA dataset was randomly categorised into two sections wherein CRL signatures were built for a training group; the accuracy of the signature was examined by a test group. Risk score = expression AP001021.1*-1.26260271849183+ expression AC105398.1*-2.41683769450866+ expression AL590434.1*-1.44825743869595+ expression AC092718.4*0.391711856978335+ expression AL050343.2*-0.554453646435766. All pictures were drawn in R (version 4.2.1), and 10 packages were used ("limma", "ggplot2", "ggalluvial", "survival", "caret", "glmnet", "survminer", "timeROC", "tidyverse", and "ggExtra").

Examination of the risk prognosis model

The Kaplan–Meier method was used to determine the OS of patients in the two risk cohorts and multiple clinical cohorts. The risk model accuracy and CRL prognostic value were validated using the Receiver Operating Characteristic (ROC), the Area Under the Curve (AUC), and the C-index curve analyses and Principal Component Analysis (PCA). Additionally, the independent prognostic factors in the risk model were explored using Uni-Cox and multivariate Cox analyses. Finally, a nomogram was used to predict the 1-, 3-, and 5- year OS with the risk model, and calibration was applied to test the accuracy of the nomogram prediction. R packages ("survival", "survminer", "timeROC", "rmc", "pec", "regplot", and "scatterplot3d") were used.

Gene Ontology (GO) and Kyoto Encyclopedia of Genes and Genomes (KEGG) analyses

R software was employed for GO and KEGG (false discovery rate <0.05) analyses between the two risk groups using the "clusterProfiler", "enrichpiot", "circlize", "R Color Brewer", and "Complex Heatmap" packages. GO comprises biological processes, cellular components, and molecular functions.

Cell culture

The MCF-7 cell line was procured from Shanghai Biowing, Ltd. (China). The MDA-MB-231 cell line was procured from Procell Life Science & Technology Co., Ltd. (China). MCF-10A was provided by a senior. The MCF-7 and MDA-MB-231 cell lines were cultured in Dulbecco's Modified Eagle Medium (Gibco, USA) and 10% fetal bovine serum (Cell-box, China) at 37°C and supplied under 5% carbon dioxide in a cell incubator. MCF-10A was cultured in a special medium (Procell, China).

Quantitative real-time Reverse Transcription (qRT)-Polymerase Chain Reaction (PCR) analysis

The medium was replaced after elesclomol (1 μM copper (II) chloride with medium) pulse treatment for 2 h. After 24 h, the total RNA was extracted using TRIzol (Tiangen). Complementary Deoxyribonucleic Acid (cDNA) was obtained using the HisScript® III 1st Strand cDNA Synthesis Kit (Vazyme, China). qRT-PCR was performed using the ChamQ Universal SYBR qPCR Master Mix (Vazyme, China). Finally, the $2^{-\Delta\Delta Ct}$ algorithm was applied to calculate relative CRL expression. The sequences of the primers used are presented in Supplementary Table 1.

Statistical analysis

The images were obtained using R (v4.2.1) software. All programs were run using Perl (5.30.0.1) software. A two-tailed Student's t-test was used to compare the control group and the experimental group. Statistical significance was set at p<0.05.

Supplementary Table 1: Sequences of CRL primers.

LncRNA	Forward primer	Reverse primer
AC092718.4	CGAAAACCTTGCCAAACCAGT	ACAGGAAGAGTTGTGGGCATT
AC105398.1	ATCCGGAATGATCAGCCATCG	AGGGAGACCAGAAAAATGCCAC
AL050343.2	TAAGGGGCTCTGGATCATGGA	CTTTGTGGAGGGCCTGAGAG
AL590434.1	GATCCTGAGACGAGACCAAGC	ACAGCGACCGAACAATAGGAA
AP001021.1	AACCCACAGCCATGGATCAAG	ATTTGCAGAGCACCAGGCTTA
GAPDH	GCACCGTCAAGGCTGAGAAC	TGGTGAAGACGCCAGTGGA

Results

Identification of prognostic CRLs

Coexpression analysis for BRCA was used to screen 268 CRLs and 14 CRGs (Figure 1A). Nine CRLs were subjected to the LASSO-Cox analysis to determine the CRL characteristics (Figure 1B, 1C). Twelve CRLs were considered statistically significant based on the Uni-Cox analysis (Figure 1D). The correlations between seven CRGs and 12 CRLs are presented in Supplementary Table 2. The heatmap in Figure 1E highlights five CRLs based on the multivariate Cox analysis (AC092718.4, AC105398.1, AL050343.2, AL590434.1, and AP001021.1).

Creation of a CRL risk prognostic model

TCGA-BRCA data were randomly divided into two cohorts (training and test groups). The training and test groups comprised 541 and 540 patient samples, respectively. According to the median expression of the risk score, each group was separated into high- and low-risk groups to conduct the follow-up experiments (Supplementary Table 3). First, each patient's risk score (Figures 2A-2C) and survival time (Figures 2D-2F) were presented for the two risk groups. Second, a heatmap demonstrated the expressions of the five CRLs in the two risk cohorts. In the low-risk group, AP001021.1, AC105398.1, AL590434.1, and AL050343.2 were highly expressed, whereas AC092718.4 had a lower expression (Figures 2G-2I). Third, the results revealed a shorter OS in the high-risk group (Figures 2J-2L). In conclusion, our prognostic model was successfully constructed, with the high-risk group having a poor prognosis than the low-risk group.

Assessment of BRCA risk score and clinical outcomes

The significance of the clinical indicators was predicted using Uni-Cox and multivariate Cox regression analyses. The former reported that five indicators, including age, stage, T classification, N classification, M classification, and risk score, were strongly significant (Figure 3A). Multivariate Cox regression revealed that the p-value was <0.001 for age and risk score; however, it was >0.05 for T, N, and M classifications (Figure 3B). The accuracy of the model's predictability was analysed using ROC and C-index curves. AUC and C-index curves confirmed the accuracy of prediction for six targets, namely risk score, age, stage, T classification, N classification, M classification, ER status, PR status and Her2 status (0.647, 0.847, 0.696, 0.723, 0.564, 0.655, 0.540, 0.566 and 0.569, respectively) (Figure 3C, 3D). The AUCs at 1, 3, 5, 8, and 10 years were 0.711, 0.647, 0.648, 0.633, and 0.617 in the entire set; 0.727, 0.702, 0.737, 0.725, and 0.692 in the training set; 0.683, 0.594, 0.594, 0.594, and 0.577 in the test set respectively (Figures 3E-3G). A nomogram presenting four clinical features and risk scores evaluated the survival time (at 1 year, 3 years, and 5 years) of patients with BRCA. The score of patients with BRCA was 253, and the 1-year, 3-year, and 5-year survival probabilities were 97.2%, 83.9%, and 71.1%, respectively (Figure 3H). Finally, the calibration picture revealed the accuracy of the estimated nomogram-predicted OS (Figure 3I). Thus, age and risk score could serve as independent prognostic factors.

Supplementary Table 2: Correlation between 7 CRGs and 12 CRLs.

CRGs	LncRNA	Cor	P value	Regulation
FDX1	AL590434.1	0.69883946	5.63E-162	positive
GCSH	AP001021.1	0.45964478	1.35E-58	positive
GCSH	AP002026.1	0.45154041	2.29E-56	positive
GCSH	AL050343.2	0.45332844	7.47E-57	positive
GLS	AP001021.1	0.489832	1.89E-67	positive
GLS	AL117335.1	0.46643021	1.65E-60	positive
GLS	AC105398.1	0.63010866	9.14E-123	positive
GLS	LINC01152	0.48802993	6.78E-67	positive
LIAS	AC092794.1	0.45144784	2.43E-56	positive
LIPT2	AP002340.1	0.65453448	1.59E-135	positive
NLRP3	LINC01366	0.47857096	4.83E-64	positive
NLRP3	AL109741.1	0.50788222	3.50E-73	positive
PDHA1	AC092718.4	0.46061228	7.25E-59	positive

Supplementary Table 3: Clinical features of patients in the training group and test group.

Covariates	Type	Total (n=1071)	Test (n=540)	Training (n=531)	P value
Age	≤ 65	765 (70.77%)	380 (70.37%)	385 (71.16%)	0.8257
	>65	316 (29.23%)	160 (29.63%)	156 (28.84%)	
Stage	Stage I	182 (16.84%)	86 (15.93%)	96 (17.74%)	0.2225
	Stage II	611 (56.52%)	321 (59.44%)	290 (53.6%)	
	Stage III	245 (22.66%)	112 (20.74%)	133 (24.58%)	
	Stage IV	19 (1.76%)	8 (1.48%)	11 (2.03%)	
	Unknown	24 (2.22%)	13 (2.41%)	11 (2.03%)	
T	T1	279 (25.81%)	134 (24.81%)	145 (26.8%)	0.4146
	T2	623 (57.63%)	322 (59.63%)	301 (55.64%)	
	T3	138 (12.77%)	68 (12.59%)	70 (12.94%)	
	T4	38 (3.52%)	15 (2.78%)	23 (4.25%)	
	Unknown	3 (0.28%)	1 (0.19%)	2 (0.37%)	
M	M0	899 (83.16%)	445 (82.41%)	454 (83.92%)	0.4165
	M1	21 (1.94%)	8 (1.48%)	13 (2.4%)	
	unknown	161 (14.89%)	87 (16.11%)	74 (13.68%)	
N	N0	330 (30.53%)	159 (29.44%)	171 (31.61%)	0.131
	N0 (i)	181 (16.74%)	97 (17.96%)	84 (15.53%)	
	N1	355 (32.84%)	184 (34.07%)	171 (31.61%)	
	N2	119 (11.01%)	60 (11.11%)	59 (10.91%)	
	N3	76 (7.03%)	28 (5.19%)	48 (8.87%)	
	Unknown	20 (1.85%)	12 (2.22%)	8 (1.48%)	

PCA and functional annotation analysis

PCA suggested four components for the high- and low-risk subgroups, which were as follows: All genes (Figure 4A), CRGs (Figure 4B), CRLs (Figure 4C), and risk lncRNAs (Figure 4D). As shown in Figure 4D, the risk lncRNAs constructed for the two risk groups could distinctly distinguish the two cohorts. The KEGG pathway analysis revealed cholesterol metabolism, complement and coagulation cascades, the Peroxisome Proliferator-Activated Receptor (PPAR) signalling pathway, and the Wnt signalling pathway (Figure 4E, 4F). GO analysis revealed that the CRLs were related to multiple biological functions, such as signalling receptor activator activity, basement membrane activity, leukocyte migration, and extracellular structural organization (Figure 4G, 4H and Supplementary Figure 1).

Exploration of the immune landscape in the high- and low-risk groups

We observed that CRLs and immune cells, including naive B cells, plasma cells, resting memory Cluster of Differentiation (CD) 4 T cells,

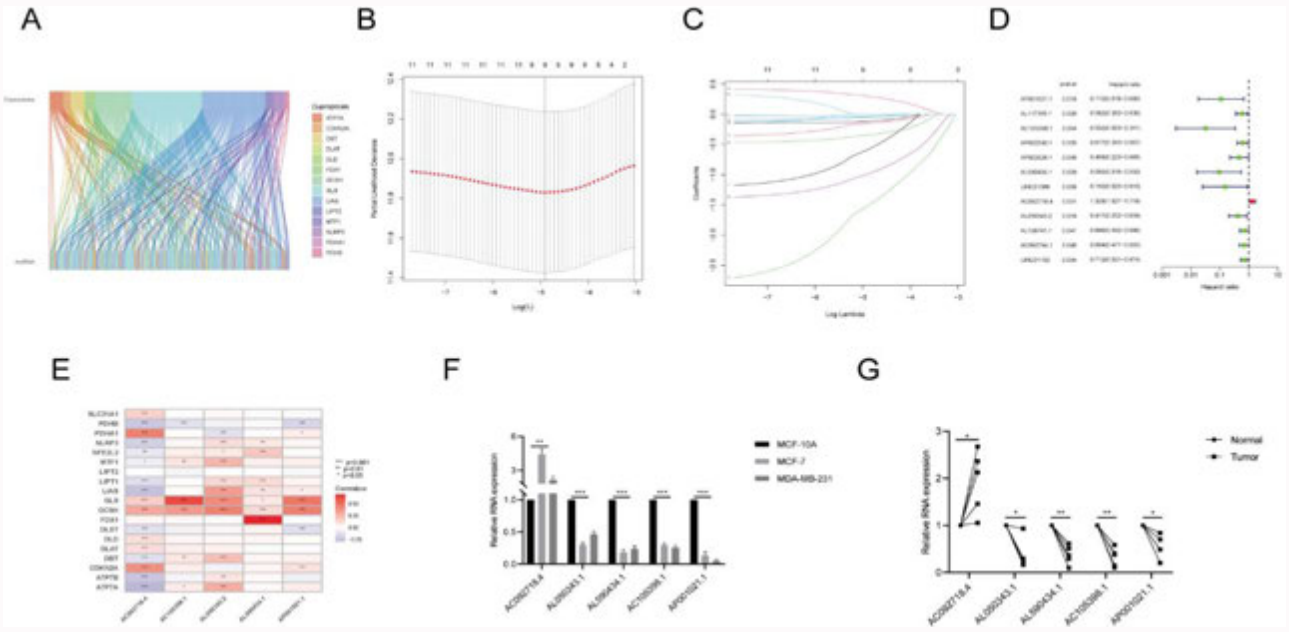

Figure 1: Screening of prognostic CRLs. (A) Sankey Diagram of the correlation between 268 CRLs and 14 CRGs. (B and C) the distribution of CRLs screened by Lasso-Cox regression analysis. (D) The forest diagram of 12 prognostic CRLs screened by univariate Cox regression analysis. (E) The heatmap of 19 prognostic CRLs and 14 CRGs. (F and G) Five CRLs expression in cell lines and paired clinical tissues.

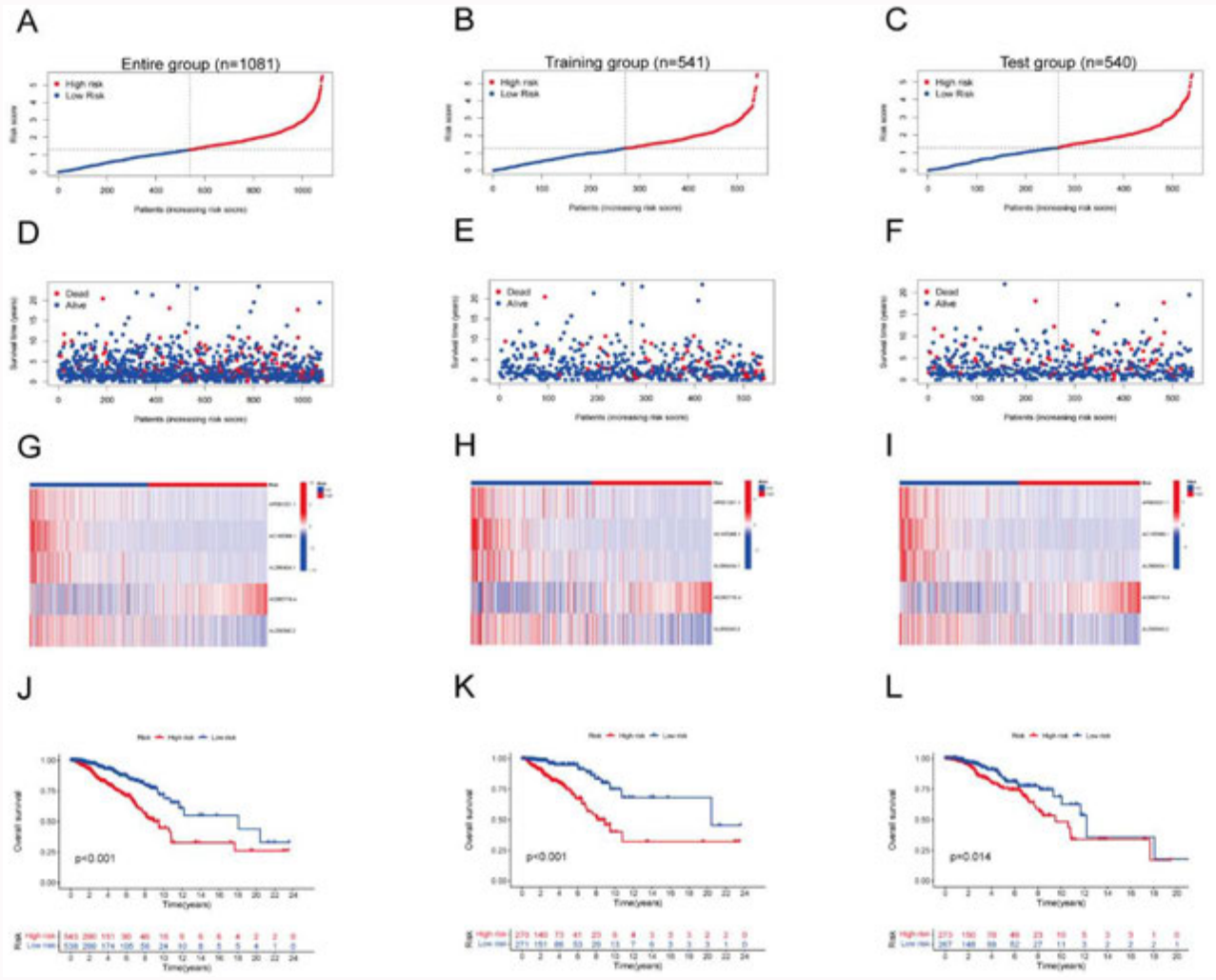

Figure 2: Construction of the prognostic risk model using the three groups. Risk scores in the high-risk and low-risk cohorts in the total group (A), training group (B) and test group (C). Survival time in the total group (D), training group (E) and test group (F). Heatmap of five CRLs in the high- and low-risk groups in the total group (G), training group (H) and test group (I). Kaplan–Meier curves for overall survival in the total group (J), training group (K) and test group (L).

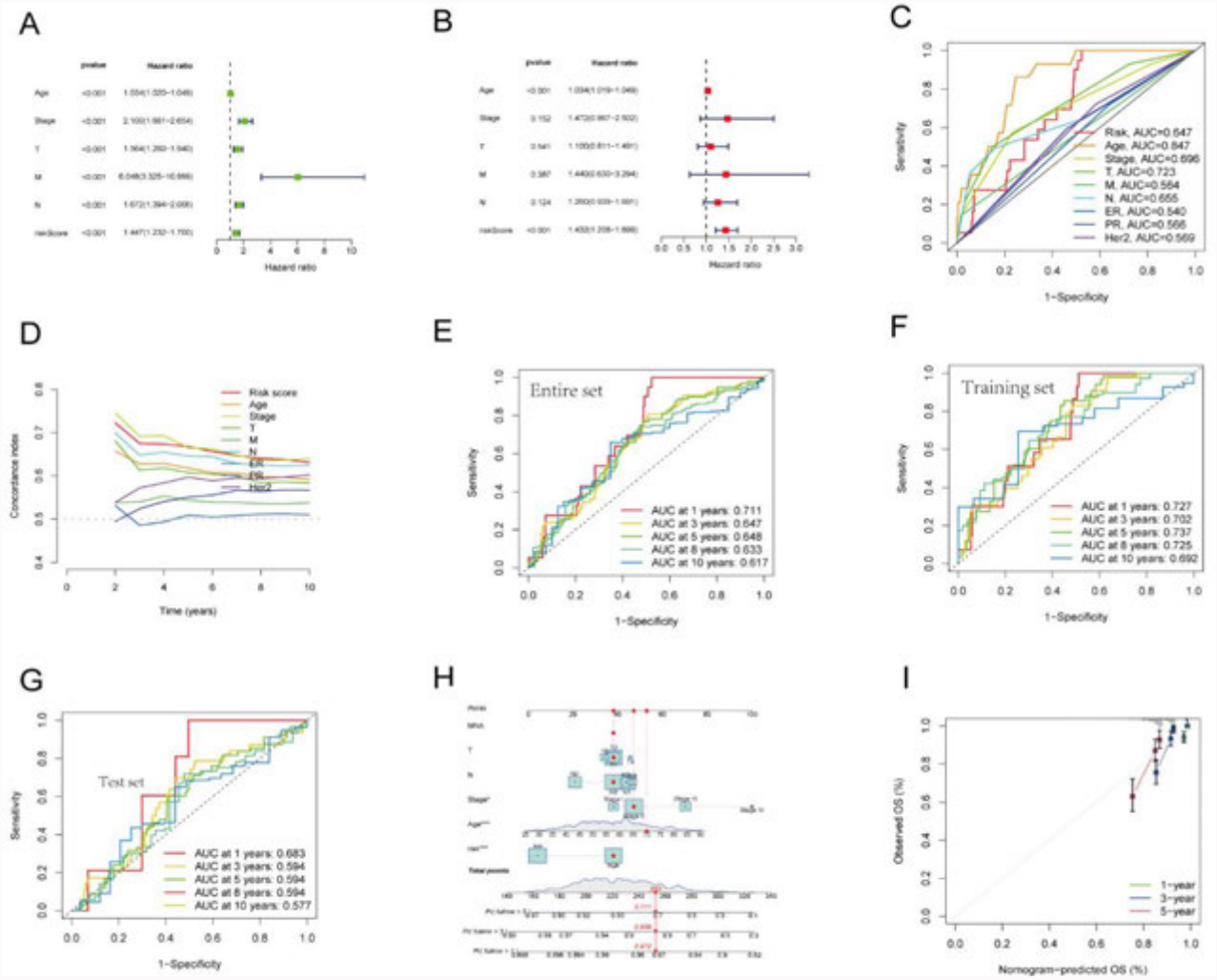

Figure 3: Prognostic evaluation of multiple clinical characteristics. Age, Stage, T classification, N classification, M classification and Risk Score were predicted by using univariate Cox analysis (A) and multivariate Cox analysis (B). (C, D) The ROC curve and C-index of clinical features. The accuracy of the model prediction by ROC curve in entire set (E), training set (F), Test set (G). (H, I) The nomogram predicted prognosis, and calibration tested the accuracy of prediction.

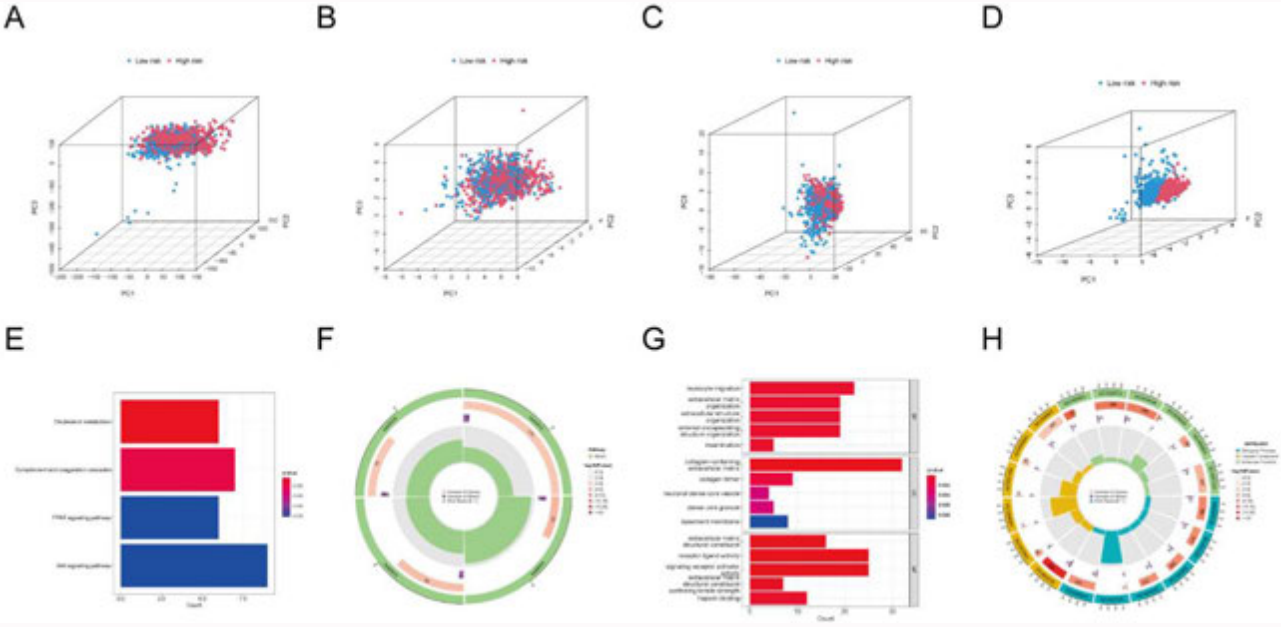

Figure 4: PCA and functional annotations of high- and low-risk groups in four cohorts. (A) All genes. (B) CRGs. (C) CRLs. (D) Risk lncRNAs. Bar plot of (E) KEGG and (G) GO pathway analyses. Loop diagram of (F) KEGG and (H) GO pathway analyses.

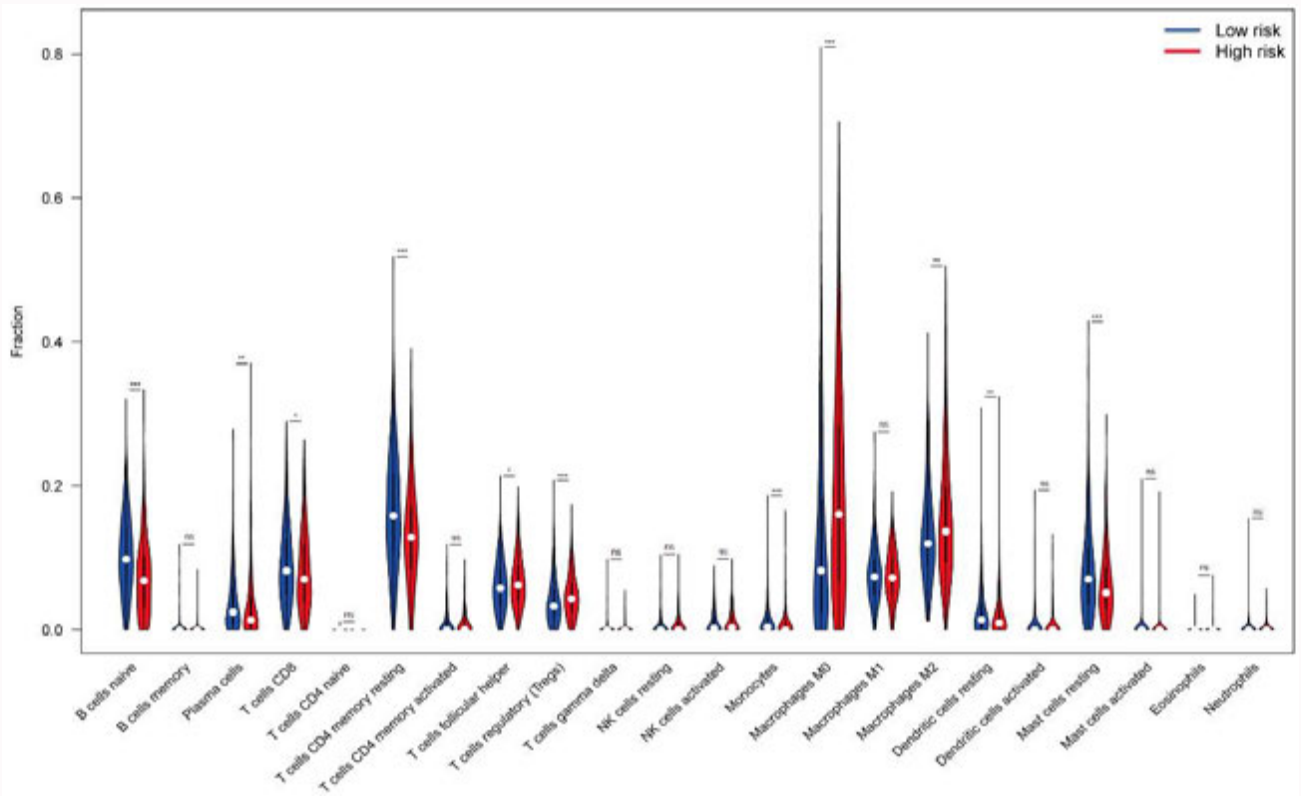

Figure 5: The fraction of 22 immune cells between the two risk cohorts.

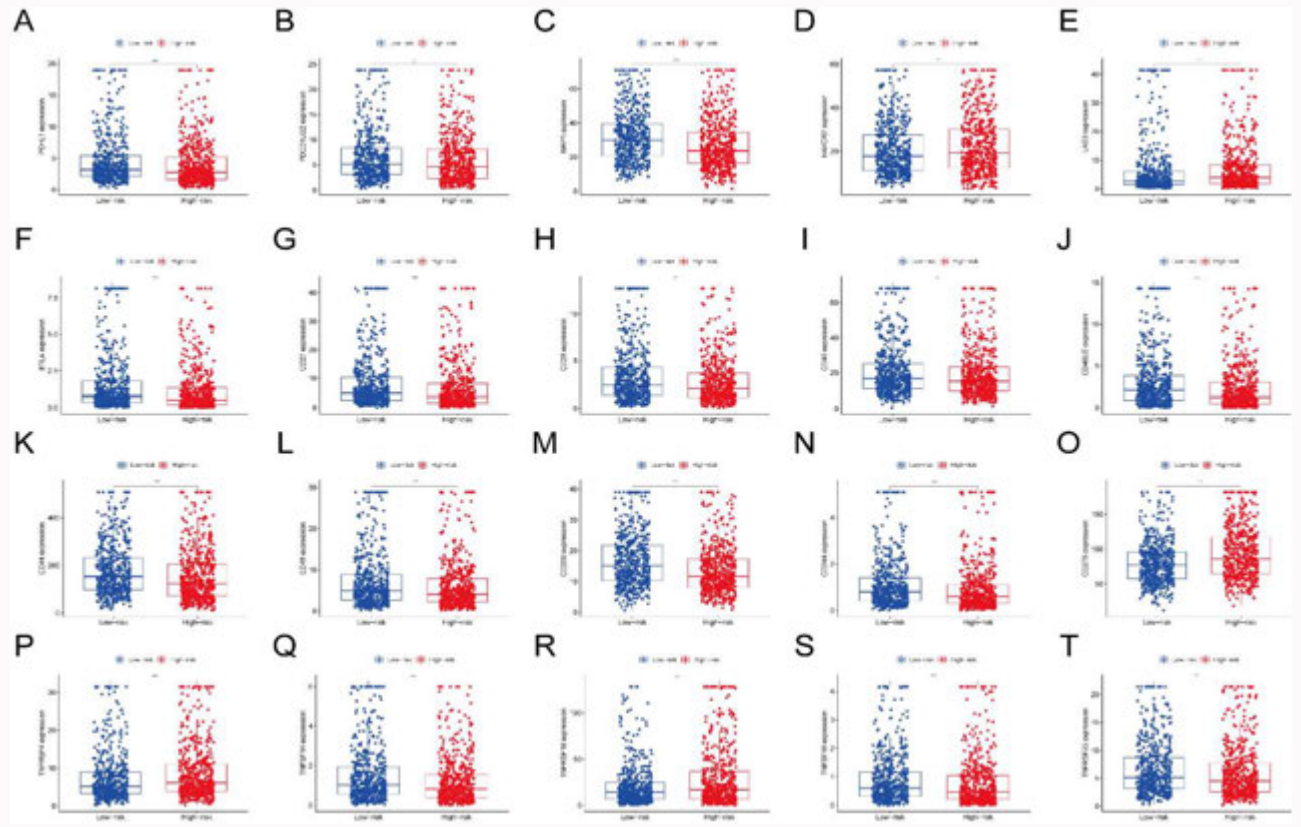

Figure 6: Expression of 20 immune checkpoints in the high- and low-risk cohorts. (A) *PD-L1*. (B) *PDCD1LG1*. (C) *NRP1*. (D) *HAVCR2*. (E) *LAG*. (F) *BTLA*. (G) *CD27*. (H) *CD28*. (I) *CD40*. (J) *CD40LG*. (K) *CD44*. (L) *CD48*. (M) *CD200*. (N) *CD244*. (O) *CD276*. (P) *TNFRSF4*. (Q) *TNFSF14*. (R) *TNFRSF18*. (S) *TNFSF18*. (T) *TNFRSF25*.

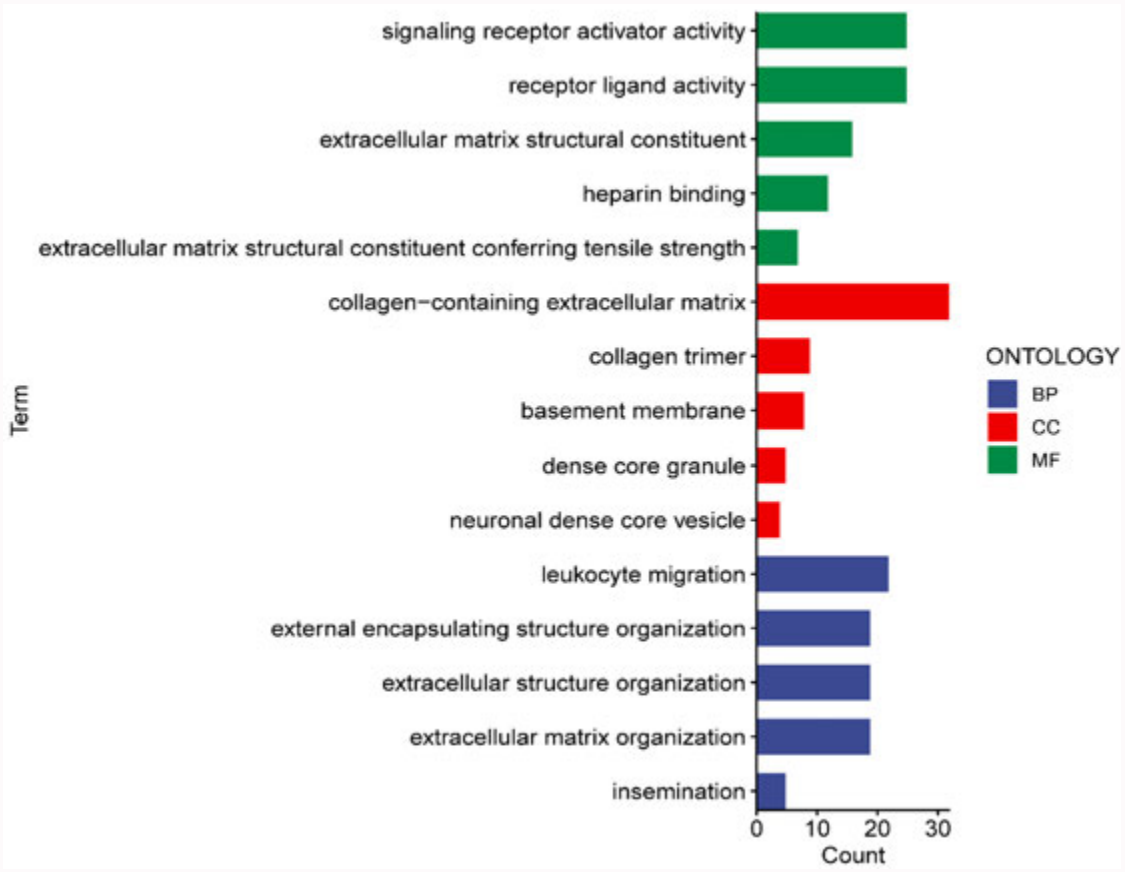

Supplementary Figure 1:

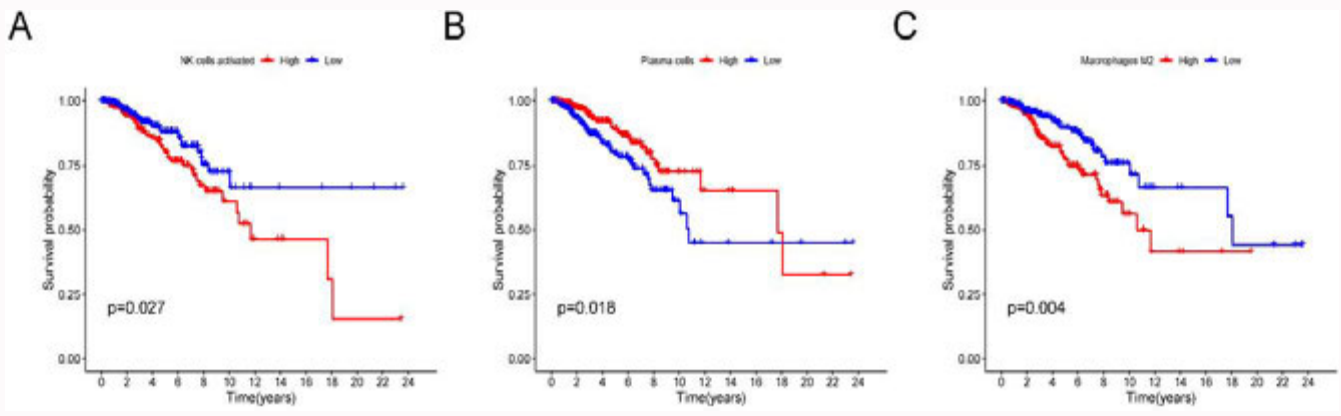

Supplementary Figure 2:

follicular helper T cells, regulatory T cells (Tregs), monocytes, M0 macrophages, M2 macrophages, resting dendritic cells, and resting mast cells, had strong internal connections in the two risk groups, as presented in Figure 5. Additionally, the OS associated with the three immune cell types was statistically significant (Supplementary Figure 2) (activated Natural Killer [NK] cells [p=0.027], plasma cells [p=0.018], and M2 macrophages [p=0.004]). Following this, we evaluated the expression of 20 immune checkpoints in the high- and low-risk groups (Figure 6). Five indicators (Hepatitis A Virus Cellular Receptor 2 [HAVCR2], Lymphocyte-Activation Gene 3 [LAG3], CD276, Tumour Necrosis Factor Receptor Superfamily [TNFRSF4], and TNFRSF18) were more highly expressed in the high-risk group than in the low-risk group. The others, including programmed death ligand 1, programmed cell death 1 ligand 2, neuropilin-1, B- and T-lymphocyte attenuator, CD27, CD28, CD40, CD40 ligand, CD44, CD48, CD200, CD244, Tumour Necrosis Factor Super Family member [TNFSF] 14, TNFSF18, and TNFRSF25, showed the opposite trend. In conclusion, we observed that CRLs were strongly associated with immune cells and immune checkpoints.

Discussion

BRCA is one of the most common malignant tumours with high incidence and mortality among women worldwide [1]. Approximately one-third of patients experience recurrence and other metastatic

diseases [14]. Tsvetkov et al. reported cuproptosis, a new type of cell death [8]. Copper can reportedly overcome tumour cell resistance to chemotherapy, inhibits cell growth, and significantly improves the survival time of tumour-bearing mice [15]. Increasing evidence has suggested that lncRNAs play a crucial role in tumour occurrence and development and participate in immune system regulation [16]. Notably, the mechanism of CRLs in tumours remains unclear, particularly in BRCA. Thus, the discovery of CRLs might provide a new therapeutic opportunity for patients with BRCA.

We first identified 268 CRLs in this study. Subsequently, we determined five prognostic CRLs (AC092718.4, AC105398.1, AL050343.2, AL590434.1, and AP001021.1) through Uni-Cox and LASSO-Cox analyses. AC092718.4 was found to be a high-risk lncRNA, whereas AC105398.1, AL050343.2, AL590.434.1, and AP001021.1 were low-risk lncRNAs. Lin et al. [17] reported that AC092718.4 is strongly associated with a dysregulation in ovarian cancer, and elevated AC092718.4 expression is associated with a poor prognosis. Compared with normal breast tissue, AC092718.4 is highly expressed in BRCA tissue and was positively associated with T and B cells [18]. The remaining four CRLs have not been reported. We predicted that five lncRNAs were positively relevant to their adjacent genes, including *FDX1*, Glycine Cleavage System Protein H [GCSH], Glutaminase [GLS], Lipoic Acid Synthetase [*LIAS*], Lipoyl (Octanoyl) Transferase 2 [LIPT2], Nucleotide-binding and Leucine-Rich Repeat Family Pyrin domain containing 3 [*NLRP3*], and Pyruvate Dehydrogenase E1 Subunit Alpha 1 [PDHA1]. *FDX1* and *LIAS* are key genes for copper ionophore-induced cell death, and *FDX1* and/or *LIAS* knockdown can protect cells from copper toxicity [8]. *FDX1* improves cancer-targeted drug efficacy and the inhibitory effect of proteasome inhibitors on cancer cells [19]. In BRCA cells, the GCSH three-dimensional Tumour volume (Tv) 1/Tv* transcript ratio ranges between 5 and 10, whereas it is 1 in normal breast cells. Tv1 overexpression could increase tumour cell viability [20]. GLS is carcinogenic and is up-regulated in pancreatic ductal adenocarcinoma to promote tumour proliferation [21]. LIPT2 mutation could result in mitochondrial lipoylation defects [22]. *NLRP3* is a pyroptosis-related gene. *NLRP3* inflammasome activation and its related molecular regulatory signalling pathways are closely associated with the occurrence and development of various diseases and is a crucial subject in clinical drug research and development [23]. Chen et al. [24] reported that PDHA1 promotes prostate cancer development *in vivo* in human and mouse prostate cancer models. A considerable number of the seven genes with partial functions have been reported in the literature; however, CRLs with these genes have rarely been studied. Thus, further details about CRLs need to be elucidated.

We first divided the TCGA-BRCA dataset into the training and test groups and constructed a prognostic risk model to further study CRLs. The data revealed that the model could predict the OS of the two risk groups. Next, Uni-Cox and multivariate Cox analyses revealed that age and the risk score could serve as independent prognostic factors. The accuracy of predicting the age and risk score was >70% according to the ROC and C-index curves. Furthermore, a nomogram was established to explore the 1-, 3-, and 5-year survival time of the patients in the two risk cohorts, and the calibration plot demonstrated excellent accuracy. Second, GO revealed the CRLs to be enriched in multiple biological functions, including immune-related functions. The KEGG analysis revealed that the CRLs were involved in cholesterol metabolism, complement and coagulation cascades, the PPAR signalling pathway, and the Wnt signalling pathway. Third, the correlation between the model and immune microenvironment was studied and observed significant differences in naive B cells, resting memory CD4 T cells, monocytes, M0 macrophages, and resting mast cells. Five immune checkpoints (HAVCR2, LAG3, CD276, TNFRSF4, and TNFRSF18) exhibited higher expression in the high-risk group than in the low-risk group. Liong et al. [25] reported that viruses could induce HAVCR2 to regulate cytokines, chemokines, prostaglandins, and cell adhesion molecules. After anti-programmed cell death protein 1 treatment, HAVCR2 and LAG3 follow clonal expansion in certain CD8+ T cells in TNBC [26]. A similar study revealed that CD276, a potential immune checkpoint member, is overexpressed in >70% of BRCA cases and that CD276 overexpression is associated with poor prognosis [27]. The high Treg_C4_TNFRSF4 cell proportion with activation potential in nasopharyngeal carcinoma has a strong immunosuppressive function [28]. TNFRSF18 ligand can bind T cell receptors to activate the mitogen-activated protein kinase/extracellular signal-regulated kinase and nuclear factor kappa-light-chain-enhancer of activated B pathways, up-regulate the immune system and enhance the antitumour effect [29]. Next, we observed that the high CRL expression in activated NK cells and M2 macrophages were associated with poor prognosis; however, contradictory results were observed for plasma cells. Recent literature suggests that a high TMB might produce new and more immunogenic neoantigens, which might be effective for immunotherapy [30]. Next, we verified the expression of the five CRLs using qRT-PCR in MCF-7 and MDA-MB-231 cells. Last, we observed that CRLs are strongly associated with six cancer types, including soft tissue sarcoma, cutaneous melanoma, hepatocellular carcinoma, osteosarcoma, colon adenocarcinoma, and head and neck squamous cell carcinoma [31-37]. Taken together, the constructed risk model could be used to evaluate patient prognosis.

Our study has a few limitations. First, all the data were obtained from a public database, which might only apply to specific populations and the correlation coefficient, was different when screening CRLs, which might lead to varied final screening results. Second, the data were obtained from TCGA, and further experimental verification *in vivo* and *in vitro* is warranted.

Conclusion

We constructed a CRL signature to provide a prediction tool for BRCA patients. This model proved that tumour microenvironment is associated with immune function and drug sensitivity. We demonstrated that five CRLs were tumour specific, and they maybe become potential therapeutic targets.

Funding

The research was supported by the National Natural Science Foundation of China (grant number: 8197102168).

Acknowledgement

We appreciate the support of Shandong Provincial Hospital. We thank Bullet Edits Limited for editing the language of the manuscript.

References

1. Siegel RL, Miller KD, Fuchs HE, Jemal A. Cancer statistics. CA Cancer J Clin. 2022;72(1):7-33.

2. Waks AG, Winer EP. Breast cancer treatment a review. JAMA. 2019;321(3):288-300.

3. Pondé NF, Zardavas D, Piccart M. Progress in adjuvant systemic therapy

for breast cancer. Nat Rev Clin Oncol. 2019;16(1):27-44.

4. Su S, Song E. The systemic effect of type 1 interferon responsiveness on tumor immunotherapy. Nat Immunol. 2022;23(8):1141-3.
5. Li ZQ, Seehawer M, Polyak K. Untangling the web of intratumour heterogeneity. Nat Cell Biol. 2022;24(8):1192-201.
6. Cobine PA, Brady DC. Cuproptosis: Cellular and molecular mechanisms underlying copper-induced cell death. Mol Cell. 2022;82(10):1786-7.
7. Li SR, Bu LL, Cai LL. Cuproptosis: Lipoylated TCA cycle proteins-mediated novel cell death pathway. Signal Transduct Target Ther. 2022;7(1):158.
8. Tsvetkov P, Coy S, Petrova B, Dreishpoon M, Verma A, Abdusamad M, et al. Copper induces cell death by targeting lipoylated TCA cycle proteins. Science. 2022;75(6586):1254-61.
9. Xiong X, Huang KB, Wang Y, Cao B, Luo Y, Chen H, et al. Target profiling of an iridium (III)-based immunogenic cell death inducer unveils the engagement of unfolded protein response regulator BiP. J Am Chem Soc. 2022;144(23):10407-16.
10. Borsani G, Tonlorenzi R, Simmler MC, Dandolo L, Arnaud D, Capra V, et al. Characterization of a murine gene expressed from the inactive X chromosome. Nature. 1991;351(6324):325-9.
11. Singh D, Assaraf Y, Gacche RN. Long non-coding RNA mediated drug resistance in breast cancer. Drug Resist Update. 2022;63:100851.
12. Statello L, Guo CJ, Chen LL, Huarte M. Gene regulation by long non-coding RNAs and its biological functions. Nat Rev Mol Cell Biol. 2021;22(2):96-118.
13. Du G, Sun J, Li Z, Zhang Q, Liu W, Yang C, et al. A feedforward circuit between KLF5 and lncRNA KPRT4 contributes to basal-like breast cancer. Cancer Lett. 2022;534:215618.
14. Martín M, Zielinski C, Ruiz-Borrego M, Carrasco E, Ciruelos EM, Muñoz M, et al. Overall survival with palbociclib plus endocrine therapy versus capecitabine in postmenopausal patients with hormone receptor-positive, HER2-negative metastatic breast cancer in the PEARL study. Eur J Cancer. 2022;168:12-24.
15. Liu J, Yuan Y, Cheng Y, Fu D, Chen Z, Wang Y, et al. Copper-based metal-organic framework overcomes cancer chemoresistance through systemically disrupting dynamically balanced cellular redox homeostasis. J Am Chem Soc. 2022;144(11):4799-809.
16. Zhang N, Zhang H, Wu W, Zhou R, Li S, Wang Z, et al. Machine learning-based identification of tumor-infiltrating immune cell-associated lncRNAs for improving outcomes and immunotherapy responses in patients with low-grade glioma. Theranostics. 2022;12(13):5931-48.
17. Lin N, Lin JZ, Tanaka Y, Sun P, Zhou X. Identification and validation of a five-lncRNA signature for predicting survival with targeted drug candidates in ovarian cancer. Bioengineered. 2021;12(1):3263-74.
18. Chen Z, Feng R, Kahlert UD, Chen Z, Torres-Dela Roche LA, Soliman A, et al. Construction of ceRNA networks associated with CD8 T cells in breast cancer. Front Oncol. 2022;12:883197.
19. Tsvetkov P, Detappe A, Cai K, Keys HR, Brune Z, Ying W, et al. Mitochondrial metabolism promotes adaptation to proteotoxic stress. Nat Chem Biol. 2019;15(7):681-9.
20. Adamus A, Müller P, Nissen B, Kasten A, Timm S, Bauwe H, et al. GCSH antisense regulation determines breast cancer cells' viability. Sci Rep. 2018;8(1):15399.
21. Tong YY, Guo D, Lin SH, Liang JZ, Yang DQ, Ma CM, et al. SUCLA2-coupled regulation of GLS succinylation and activity counteracts oxidative stress in tumor cells. Mol Cell. 2021;81(11):2303-16.e8.
22. Habarou F, Hamel Y, Haack TB, Feichtinger RG, Lebigot E, Marquardt I, et al. Biallelic mutations in LIPT2 cause a mitochondrial lipoylation defect associated with severe neonatal encephalopathy. Am J Hum Genet. 2017;101(2):283-90.
23. Seoane PI, Lee B, Hoyle C, Yu S, Lopez-Castejon G, Lowe M, et al. The NLRP3-inflammasome as a sensor of organelle dysfunction. J Cell Biol. 2020;219(12):e202006194.
24. Chen J, Guccini I, Di Mitri D, Brina D, Revandkar A, Sarti M, et al. Compartmentalized activities of the pyruvate dehydrogenase complex sustain lipogenesis in prostate cancer. Nat Genet. 2018;50(2):219-28.
25. Liong S, Lim R, Barker G, Lappas M. Hepatitis A Virus Cellular Receptor 2 (HAVCR2) is decreased with viral infection and regulates pro-labour mediators OA. Am J Reprod Immunol. 2017;78(1).
26. Bassez A, Vos H, Dyck LV, Floris G, Arijs I, Desmedt C, et al. A single-cell map of intratumoral changes during anti-PD1 treatment of patients with breast cancer. Nat Med. 2021;27(5):820-32.
27. Durlanik S, Fundel-Clemens K, Viollet C, Huber HJ, Lenter M, Kitt K, et al. CD276 is an important player in macrophage recruitment into the tumor and an upstream regulator for PAI-1. Sci Rep. 2021;11(1):14849.
28. Liu Y, He S, Wang XL, Peng W, Chen QY, Chi DM, et al. Tumour heterogeneity and intercellular networks of nasopharyngeal carcinoma at single cell resolution. Nat Commun. 2021;12(1):741.
29. Loick SM, Fröhlich A, Gabrielpillai J, Franzen A, Vogt TJ, Dietrich J, et al. DNA Methylation and mRNA Expression of OX40 (TNFRSF4) and GITR (TNFRSF18, AITR) in head and neck squamous cell carcinoma correlates with HPV status, mutational load, an interferon-γ signature, signatures of immune infiltrates, and survival. J Immunother. 2022;45(4):194-206.
30. McGrail DJ, Pilié PG, Rashid NU, Voorwerk L, Slagter M, Kok M, et al. High tumor mutation burden fails to predict immune checkpoint blockade response across all cancer types. Ann Oncol. 2021;32(5):661-72.
31. Han J, Hu Y, Liu S, Jiang J, Wang H. A newly established cuproptosis-associated long non-coding RNA signature for predicting prognosis and indicating immune microenvironment features in soft tissue sarcoma. J Oncol. 2022;2022:8489387.
32. Zhou Y, Shu Q, Fu Z, Wang C, Gu J, Li J, et al. A novel risk model based on cuproptosis-related lncRNAs predicted prognosis and indicated immune microenvironment landscape of patients with cutaneous melanoma. Front Genet. 2022;13:959456.
33. Zhang G, Sun J, Zhang X. A novel Cuproptosis-related LncRNA signature to predict prognosis in hepatocellular carcinoma. Sci Rep. 2022;12(1):11325.
34. Yang M, Zheng H, Xu K, Yuan Q, Aihaiti Y, Cai Y, et al. A novel signature to guide osteosarcoma prognosis and immune microenvironment: Cuproptosis-related lncRNA. Front Immunol. 2022;13:919231.
35. Xu M, Mu J, Wang J, Zhou Q, Wang J. Construction and validation of a cuproptosis-related lncRNA signature as a novel and robust prognostic model for colon adenocarcinoma. Front Oncol. 2022;12:961213.
36. Yang L, Yu J, Tao L, Huang H, Gao Y, Yao J, et al. Cuproptosis-Related lncRNAs are biomarkers of prognosis and immune microenvironment in head and neck squamous cell carcinoma. Front Genet. 2022;13:947551.
37. Li YJ, Li HY, Zhang Q, Wei SL. The prognostic value and immune landscape of a cuproptosis-related lncRNA signature in head and neck squamous cell carcinoma. Front Genet. 2022;13:942785.